Solar Energy Materials & Solar Cells 107 (2012) 263–271

Contents lists available at SciVerse ScienceDirect

Solar Energy Materials & Solar Cells

journal homepage: www.elsevier.com/locate/solmat

Influence of the compensation level on the performance of p-type crystalline silicon solar cells: Theoretical calculations and experimental study

Chengquan Xiao, Deren Yang, Xuegong Yu *, Xin Gu, Duanlin Que

State Key Laboratory of Silicon Materials and Department of Materials Science and Engineering, Zhejiang University, Hangzhou 310027, People's Republic of China

ARTICLE INFO

Article history:
Received 23 May 2012
Received in revised form
27 June 2012
Accepted 28 June 2012
Available online 20 July 2012

Keywords:
Crystalline silicon solar cell
Compensation level
Incomplete ionization
Carrier mobility
Carrier lifetime
Cell efficiency

ABSTRACT

We have investigated the influence of the compensation level on the performance of p-type crystalline silicon solar cells by combining theoretical calculations and experiments. With the compensation level increasing, the fraction of ionized boron (B) atoms increases. The hole mobility is significantly reduced due to the increased ionized impurities scattering, while the electron mobility almost keeps constant due to the inverse contributions of ionized impurities scattering and electron–hole scattering. The carrier lifetime in compensated silicon, mainly dominated by high concentration of dopants, could get improved. Correspondingly, the minority carrier diffusion length increases, causing a higher short-circuit current. However, the open-circuit voltage first decreases and then increases with the increase of the compensation level, owing to the competition effect of the reduced net doping concentration and the increased excess carrier concentration. All these factors could finally result in a higher efficiency solar cell. These results suggest that intentional dopant compensation might be utilized for the improvement of solar cell efficiency, which is especially interesting for those based on highly-doped silicon feedstock.

1. Introduction

Low-cost upgraded metallurgical grade silicon (UMG-Si) directly purified by metallurgical routes has been used to fabricate solar cells in photovoltaic (PV) industry. However, this material usually contains certain amounts of boron (B) and phosphorus (P), which are not easily removed [1–6]. An alternative method is adding one dopant to compensate another dopant existing in UMG-Si during crystal growth in order to achieve suitable resistivity for the fabrication of solar cells. Recently, the electrical properties of compensated silicon wafers and solar cells have been investigated intensively. Due to the greater impurity scattering, dopant compensation might result in the reduction on both majority and minority carrier mobilities [7,8]. However, the minority carrier lifetime could be improved, benefiting from the dopant compensation [9,10]. This might counterbalance the detrimental influence of carrier mobility reduction, and therefore lead to some improvement in the minority carrier diffusion length. Czochralski (CZ) silicon solar cells with an efficiency of 15.1–16.7% have been obtained using the silicon feedstock consisting of 10% compensated silicon and 90% electronic grade silicon (EG-Si) [11]. Multicrystalline (mc) silicon solar cells with an efficiency of 15.9% have been obtained using highly-doped and compensated silicon feedstock [12]. Our previous study shows that a higher open-circuit voltage (V_{oc}) could be obtained from the compensated silicon solar cells due to its larger net doping concentration (p_0), and therefore the compensated silicon solar cells could have the same efficiency as the conventional ones [13]. Experimental progresses have been markedly made for the compensated silicon solar cells, however, it is not clear yet how the compensation level (C_I) affects the performance of crystalline silicon solar cells, i.e. short-circuit current (J_{sc}), V_{oc}, fill factor (FF) and cell efficiency (η). A systematic investigation and deep understanding of compensation effect in crystalline silicon are still quite necessary for the application of low-cost raw silicon materials in PV industry.

In this paper, we have demonstrated the influence of C_I on the performance of p-type crystalline silicon solar cells. It first shows the theoretically calculated results, in which the material characteristics of compensated silicon wafers and the electrical parameters of compensated silicon solar cells as a function of C_I have been described. Incomplete ionization of dopants is included in the calculations, since it has a strong influence on the electrical properties of compensated silicon wafers [14]. Then, the experimental results which confirm the theoretical calculations have been presented. These results are practically of significance for the understanding of compensation effect in crystalline silicon and its application in PV industry.

2. Theoretical calculations

The influence of C_I on the silicon material characteristics and the electrical parameters of solar cells is investigated by means of

* Corresponding author. Fax: +86 571 87952322.
E-mail address: yuxuegong@zju.edu.cn (X. Yu).

0927-0248/$ - see front matter Crown Copyright © 2012 Published by Elsevier B.V. All rights reserved.
http://dx.doi.org/10.1016/j.solmat.2012.06.046

theoretical calculations in this part. Here, C_I is defined as $(N_A+N_D)/(N_A-N_D)$, which represents how close to each other N_A and N_D are. C_I varies as a function of N_D for three fixed N_A in our study, i.e. 5×10^{16}, 1×10^{17} and 3×10^{17} cm^{-3}. It is a meaningful way to present the results, since it gives an insight of the effect of adding additional P atoms to silicon material with a given amount of B atoms, which is typical in practice. The calculations consist of two serial components: (1) material characteristics, including incomplete ionization, carrier mobility, carrier lifetime and minority carrier diffusion length; (2) electrical parameters of solar cells, including J_{sc}, V_{oc}, FF and η.

2.1. Material characteristics

2.1.1. Incomplete ionization

Incomplete ionization is usually neglected in the case of conventional solar cells made of uncompensated silicon with a relatively low doping concentration ($\sim10^{16}$ cm^{-3}). However, it would become questionable in the case of compensated silicon, where high concentration of dopants (B or P) would result in the proximity of the Fermi level E_F and the majority dopant energy (E_B in p-type silicon or E_P in n-type silicon) and thus a non-negligible fraction of unionized majority dopant. Considering the case of p-type compensated silicon in our study, a portion of B atoms are unionized, while P atoms are completely ionized since E_P is far above E_F. Based on the Fermi–Dirac statistics, the fraction of ionized B atoms can be calculated as follows:

$$\frac{[B^-]}{[B]}=\frac{1}{1+g\times\exp\left(\frac{E_B-E_F}{kT}\right)} \quad (1)$$

where $[B^-]$ and $[B]$ are the concentrations of ionized and total B atoms, respectively, g is the degeneracy factor equal to four for B, k is the Boltzman constant and T is the absolute temperature. In uncompensated silicon with a relatively low $[B]$, the value of E_B is often taken as equal to 44.4 meV. However, at high $[B]$, E_B can decrease due to the approached metal–nonmetal (MNM) transition. The variation of E_B as a function of $[B]$, shown in Fig. 1, was computed on the basis of a parameterization equation proposed by Altermatt et al. [15]. When $[B]$ increases from 5×10^{16} cm^{-3} to 3×10^{17} cm^{-3}, the value of E_B varies from 43.9 meV to 39.3 meV. It should be noted that the effect of compensation on E_B is neglected in our study. Recently, Tajima et al. [16] has shown that compensation could not change E_B in the low concentration range (1.1×10^{16}–8.1×10^{16} cm^{-3}). For higher $[B]$, since there is no available data concerning E_B, we assume that E_B is not affected by compensation, as previously considered by Veirman et al. [12] and Forster et al. [14].

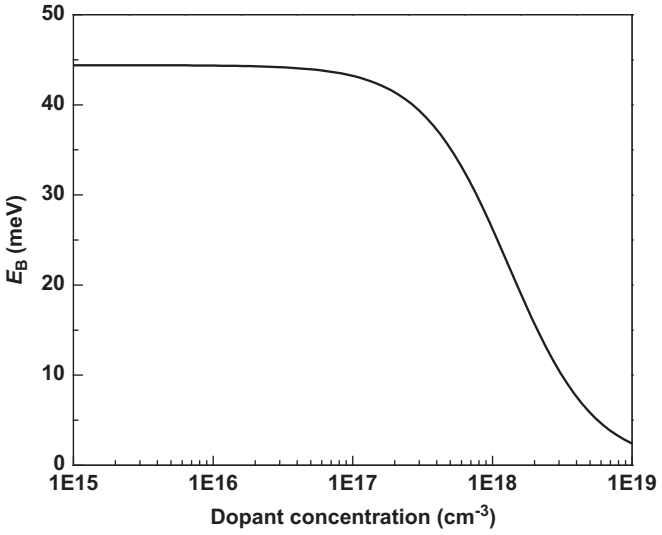

Fig. 1. Variation of the activation energy of B as a function of dopant concentration.

The p_0 can be expressed by Boltzman statistics as follows:

$$p_0=N_V\exp\left(\frac{E_V-E_F}{kT}\right) \quad (2)$$

where N_V is the effective state density in the valence band and E_V is the energy at the top of the valence band. Combining Eqs. (1) and (2), the fraction of ionized B atoms $[B^-]/[B]$ and the incomplete ionization ratio $p_0/(N_A-N_D)$ can be deduced. Fig. 2 shows the fraction of ionized B atoms, the incomplete ionization ratio and p_0 as a function of C_I for three fixed N_A. In the case of uncompensated silicon ($C_I=1$), the fraction of ionized B atoms decreases with the increase of $[B]$, which changes from 96.7% to 86.7% as $[B]$ increases from 5×10^{16} cm^{-3} to 3×10^{17} cm^{-3}. The reason is that with the increase of $[B]$, E_F gets closer to E_B and

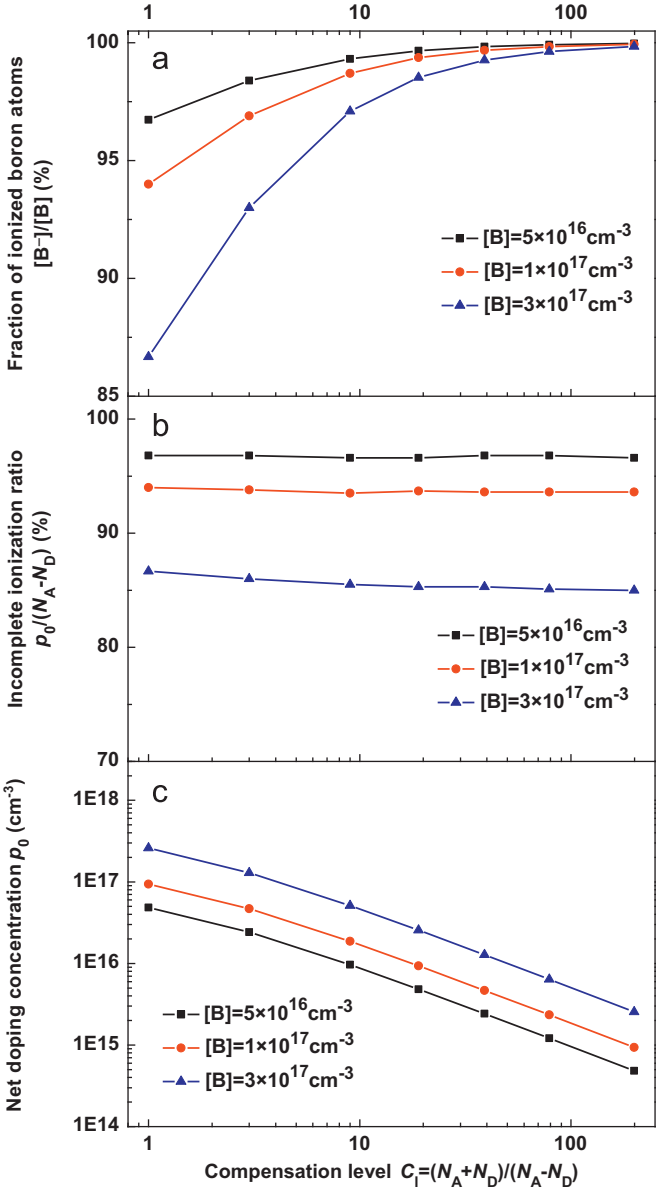

Fig. 2. Calculation of the variation of (a) the fraction of ionized B atoms $[B^-]/[B]$, (b) the incomplete ionization ratio $p_0/(N_A-N_D)$ and (c) the net doping concentration p_0 as a function of C_I for three fixed N_A, i. e. 5×10^{16}, 1×10^{17} and 3×10^{17} cm^{-3}.

therefore a larger portion of B-related shallow levels would not be occupied by electron. With C_I increasing, more and more B atoms will be compensated with P atoms, and E_F is shifted towards the middle of the gap. This would result in an increase of the fraction of ionized B atoms, see Fig. 2(a). Most of the B atoms are ionized when the value of C_I is equal to 100 for three fixed N_A. Fig. 2(b) shows the incomplete ionization ratio as a function of C_I. It can be seen that the incomplete ionization ratio almost keeps constant in the case of low [B]. However, it slightly decreases in the case of high [B]. An overestimation of p_0 would be at least 15% if incomplete ionization is neglected in the case of [B]$=3\times10^{17}$ cm^{-3}. This result implies that a small amount of unionized B atoms might have a strong influence on p_0. It suggests that incomplete ionization must be taken into account to estimate p_0 when the doping level is high. Fig. 2(c) shows the p_0 as a function of C_I for three fixed N_A. It is obvious that the p_0 investigated here is in the range of doping concentrations for photovoltaic silicon.

2.1.2. Carrier mobility

The hole and electron mobilities in silicon as a function of dopant concentration can be described by different mobility models [17–22]. Here, we use Klaassen's model [21,22] in our calculations. This model has the potential to correctly describe the carrier mobility in compensated silicon since the scattering by acceptors and donors are treated separately. Klaassen's model includes lattice scattering ($\mu_{h,L}$, $\mu_{e,L}$), ionized acceptor and donor impurities scattering ($\mu_{h,A}$, $\mu_{h,D}$, $\mu_{e,A}$, $\mu_{e,D}$) and electron–hole scattering ($\mu_{h,e}$, $\mu_{e,h}$). The total carrier mobility can be given by the sum of these terms:

$$\frac{1}{\mu_h}=\frac{1}{\mu_{h,L}}+\frac{1}{\mu_{h,A}}+\frac{1}{\mu_{h,D}}+\frac{1}{\mu_{h,e}} \tag{3}$$

$$\frac{1}{\mu_e}=\frac{1}{\mu_{e,L}}+\frac{1}{\mu_{e,A}}+\frac{1}{\mu_{e,D}}+\frac{1}{\mu_{e,h}} \tag{4}$$

Fig. 3 shows the respective contributions of lattice scattering, ionized acceptor and donor impurities scattering and electron–hole scattering on the total hole mobility as a function of C_I for three fixed N_A. Several comments can be made concerning the influence of all these scattering mechanisms on the total hole mobility. Firstly, with C_I increasing, the hole mobility limited by lattice scattering keeps constant, while the hole mobilities limited by ionized donor impurity scattering and electron–hole scattering decrease. This is because lattice scattering affects the hole mobility by means of the interaction with phonons which is only a function of the temperature, while ionized donor impurity scattering and electron–hole scattering affect the hole mobility by means of the Coulombic interaction with fixed (P^+) and moved (electrons) charges, respectively, which could grow in number with C_I increasing. Since electrons are minority carriers in p-type silicon, the effect of electron–hole scattering on the total hole mobility could be negligible, see the inset of Fig. 3(a–c). Secondly, with C_I increasing, the hole mobility limited by ionized acceptor impurity scattering also shows a slightly decrease, which is mainly attributed to the increased ionized B atoms. It should be noted that at high C_I, the contributions of ionized acceptor and donor impurities scattering on the hole mobility almost pay the

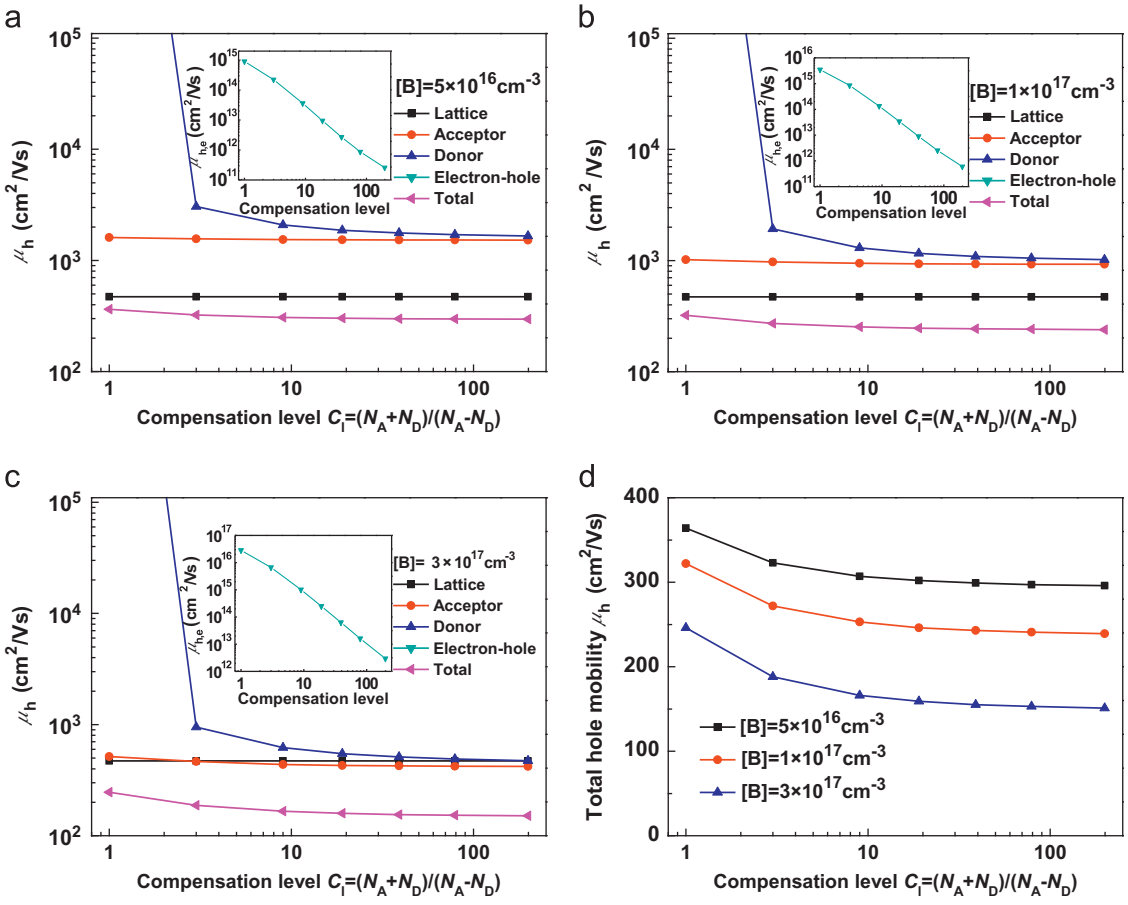

Fig. 3. Hole mobility as a function of C_I for silicon with (a) [B]$=5\times10^{16}$ cm^{-3}, (b) [B]$=1\times10^{17}$ cm^{-3} and (c) [B]$=3\times10^{17}$ cm^{-3}, the contributions of lattice scattering, ionized acceptor and donor impurities scattering and electron–hole scattering are shown. The inset of (a), (b) and (c) show the contribution of electron–hole scattering on the hole mobility for three fixed N_A. The total hole mobility as a function of C_I for three fixed N_A is shown in (d).

same role, owing to the extra-close concentrations for ionized acceptor and donor. Therefore, with the increase of C_I, the total hole mobility decreases monotonously, resulting from the increased ionized impurities scattering. Comparing the contribution of ionized impurities scattering with that of lattice scattering (constant in our study), the ionized impurities scattering could affect the total hole mobility strongly for different [B]. For instance, in the case of uncompensated silicon ($C_I=1$), the contribution of ionized impurities scattering $1/\mu_{h,A}$ on the total scattering $1/\mu_h$ increases from 22.6% to 47.7% with [B] increasing from 5×10^{16} cm^{-3} to 3×10^{17} cm^{-3}, and therefore the total hole mobility decreases from 364 cm^2/V s to 246 cm^2/V s.

Fig. 4 shows the contributions of lattice scattering, ionized acceptor and donor impurities scattering and electron–hole scattering on the total electron mobility as a function of C_I for three fixed N_A. It can be seen that the effects of lattice scattering and ionized impurities scattering on the electron mobility are almost similar with those on the hole mobility mentioned above. However, the electron–hole scattering could have a great influence on the total electron mobility. The reason is that the electron mobility limited by electron–hole scattering is mainly dependent on the amount of holes p_0 which are majority carriers in p-type silicon. With the increase of C_I, the value of p_0 decreases sharply. Correspondingly, the electron–hole scattering becomes weaker and the electron mobility limited by electron–hole scattering increases quickly, see Fig. 4(a–c). Due to the inverse contributions of electron–hole scattering and ionized impurities scattering, the total electron mobility almost keeps constant with the increase of C_I, see Fig. 4(d). The result implies that compensation would not have a significant influence on the minority carrier mobility in p-type silicon with the same [B].

2.1.3. Carrier lifetime

Generally, the minority carrier lifetime in silicon is mainly determined by the Shockley-Read-Hall (SRH) recombination through defects and impurities. Assuming the absence of carrier trapping effect, the excess electron and hole concentrations can be considered equal ($\Delta n=\Delta p$). Therefore, the minority carrier lifetime (τ) can be expressed as follows:

$$\tau=\frac{\tau_{n0}(p_0+p_1+\Delta n)+\tau_{p0}(n_0+n_1+\Delta n)}{p_0+n_0+\Delta n} \tag{5}$$

where $\tau_{n0,p0}=1/(N_T\sigma_{n,p}\nu_{th})$, N_T the concentration of the recombination centers, $\sigma_{n,p}$ the capture cross sections for electrons and holes, ν_{th} the thermal velocity, n_0 the equilibrium electron concentration, p_1 and n_1 are equal to the equilibrium hole and electron concentrations when the Fermi level coincides with the energy level of the recombination centers [23]. In reality, the minority carrier lifetime in photovoltaic silicon, is limited by the recombination through both doping species and metal impurities. Here, the effect of B and iron (Fe) on the minority carrier lifetime has been taken into account in our study. Generally, Fe atoms can either occupy interstitial lattice sites in silicon matrix or pair with substitutional B atoms under thermal equilibrium, namely FeB pairs. After a typical phosphorus diffusion gettering (PDG) step is applied, the concentration of FeB pairs in the final solar cells is usually at the level of $\sim10^{11}$ cm^{-3} [24,25]. The detailed parameters of B and FeB pairs used for calculating the minority carrier lifetime via SRH model are listed in Table 1 [9,15,26]. Therefore, the effective minority carrier lifetime can be determined by

$$\frac{1}{\tau_{eff}}=\frac{1}{\tau_B}+\frac{1}{\tau_{FeB}} \tag{6}$$

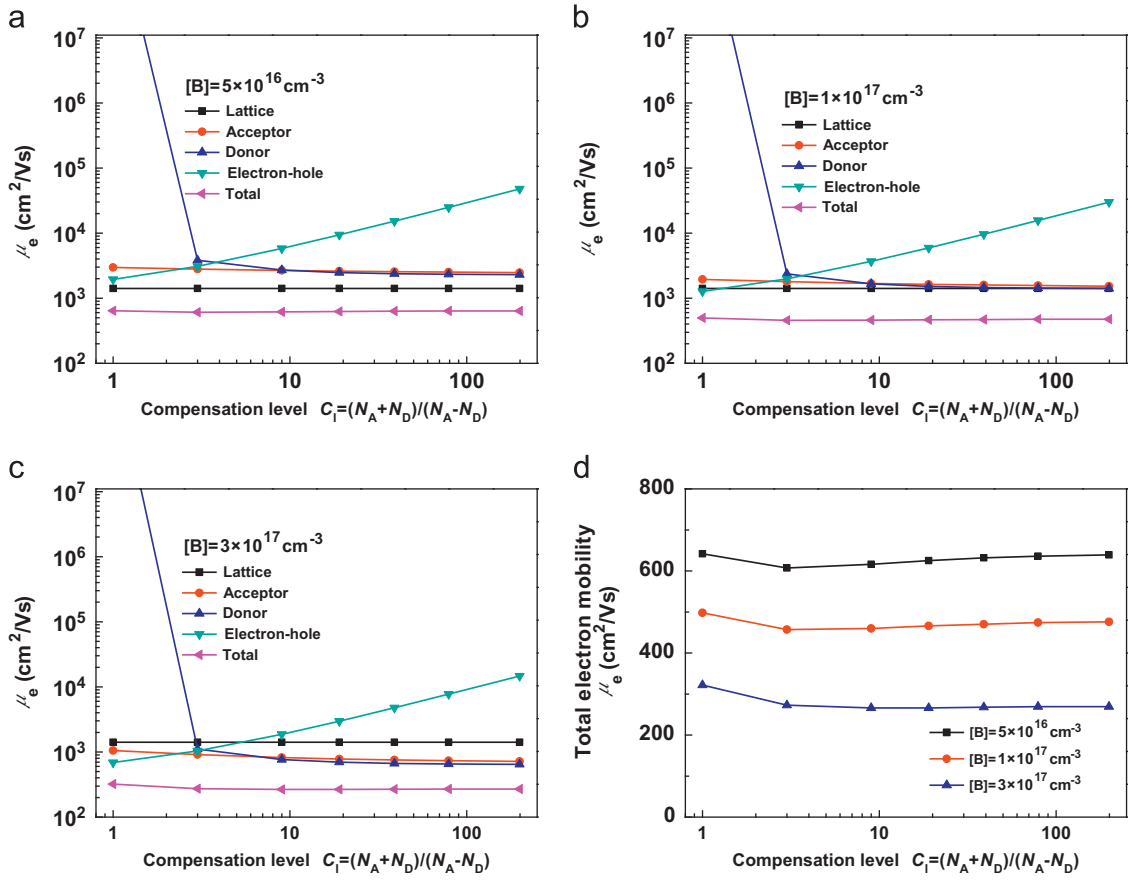

Fig. 4. Electron mobility as a function of C_I for silicon with (a) [B]$=5\times10^{16}$ cm^{-3}, (b) [B]$=1\times10^{17}$ cm^{-3} and (c) [B]$=3\times10^{17}$ cm^{-3}, the contributions of lattice scattering, ionized acceptor and donor impurities scattering and electron–hole scattering are shown. The total electron mobility as a function of C_I for three fixed N_A is shown in (d).

where τ_B and τ_{FeB} are the minority carrier lifetimes limited to B and FeB pairs, respectively. Note that in our calculations, the injection level (Δn) is set as $\sim 10^{12}\,cm^{-3}$, which corresponds to the low-injection condition. Fig. 5(a) shows the minority carrier lifetime in silicon wafer as a function of C_I in the case of $N_A = 1\times10^{17}\,cm^{-3}$. It can be seen that the minority carrier lifetimes limited by both B and FeB pairs increase with the increase of C_I. This leads us believe that dopant compensation could have a beneficial effect on the improvement of the effective minority carrier lifetime. This has been explained by the decrease of recombination strength of recombination centers, as a result of the reduction in the p_0 [9]. Besides, one can see that the effective minority carrier lifetime in silicon wafer is mainly dominated by doping species, rather than the low concentration of metal impurities after a PDG process. This result is consistent with the experimental analysis reported recently by Veirman et al. [12]. Fig. 5(b) shows the effective minority carrier lifetime in silicon wafer as a function of C_I for three fixed N_A. Obviously, the effective minority carrier lifetime could get improved due to dopant compensation. It should be mentioned that the simplified SRH statistic can only be applied for the situation that the concentration of recombination centers N_T is at least an order of magnitude lower than a critical level N_{crit}, which depends on the p_0 and the ratio of σ_p and σ_n [27]. Using the parameters of $\sigma_{n,p}$ for B and FeB pairs listed in Table 1, the values of N_{crit} are found to be $5.7\times10^{18}\,cm^{-3}$ and $1.6\times10^{15}\,cm^{-3}$ for B and FeB pairs, respectively, even at the lowest p_0 value ($4.8\times10^{14}\,cm^{-3}$) in our calculations. Thus, the simplified SRH statistic should be applicable for photovoltaic silicon.

2.1.4. Minority carrier diffusion length

For standard cells, the minority carrier diffusion length (L_{diff}) is a very important parameter influencing the cell efficiency, which can be estimated as follows

$$L_{diff} = \sqrt{D_e \tau_{eff}} \tag{7}$$

Table 1
Parameters used for SRH lifetime calculation.

	E_T(eV)	σ_n(cm^2)	σ_p(cm^2)	N_T(cm^{-3})	Ref.
B	E_v+0.039–0.044	1×10^{-17}	7.65×10^{-12}	N_A	[9,15]
FeB	E_c−0.26	5×10^{-15}	3×10^{-15}	1×10^{11}	[26]

with

$$D_e = \mu_e \frac{kT}{q} \tag{8}$$

where D_e is the electron diffusion coefficient and q the charge unit. From the results above (Section 2.1.2 and Section 2.1.3), it can be known that with the increase of C_I, the electron mobility almost keeps constant, while the effective minority carrier lifetime could get significantly improved. This could result in the increase of L_{diff}, see Fig. 6. In the case of $[B]=3\times10^{17}\,cm^{-3}$, the value of L_{diff} increases from 27.0 μm to 223.5 μm when C_I increases from 1 to 199. It is known that the UMG-Si solar cells generally suffer from the low minority carrier diffusion length, which is usually less than the thickness of solar cell [9]. Here, dopant compensation could supply an effective way to the improvement of L_{diff} for the UMG-Si solar cells.

2.2. Solar cell parameters

The electrical parameters (J_{sc}, V_{oc}, FF and η) of the corresponding solar cells are simulated with PC1D [28]. Notice that PC1D is a software developed for uncompensated materials. The p_0 is assumed equal to the base doping concentration [B] in PC1D. Consequently, the carrier mobilities are calculated automatically from the [B] value through the Arora's model [17]. Fortunately,

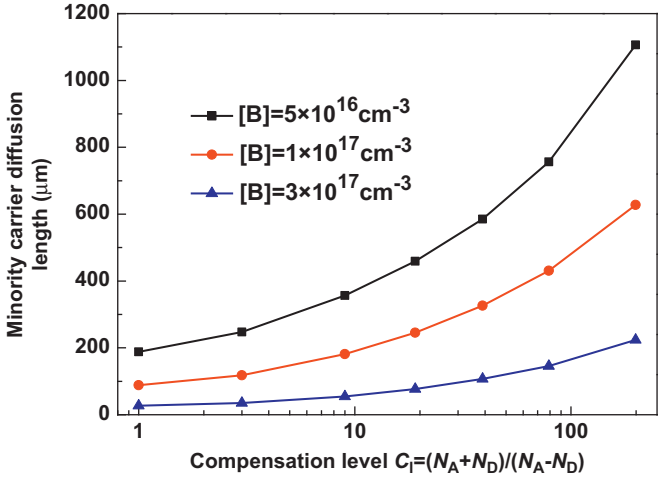

Fig. 6. Minority carrier diffusion length in silicon wafer as a function of C_I for three fixed N_A.

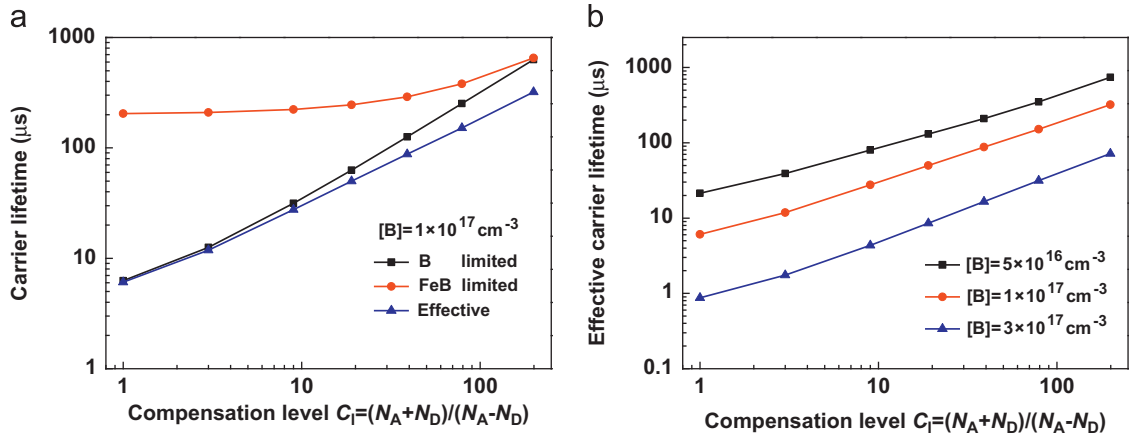

Fig. 5. (a) Carrier lifetime in silicon wafer limited by the recombination of both B and FeB pairs as a function of C_I in the case of $[B]=1\times10^{17}\,cm^{-3}$ and (b) effective carrier lifetime in silicon wafer as a function of C_I for three fixed N_A.

it is allowed to enter our own values of μ and p_0 (computed by taking into account the incomplete ionization of the B atoms). Therefore, in our simulation, we enter our own values of μ, p_0 and L_{diff} for each compensation level in PC1D. For obtaining the simulated results, a wafer thickness of 200 μm and an area of 148.55 cm^2 were assumed, together with a silicon nitride antireflection coating on the front textured surface. As for surface recombination, the front and rear surfaces were modeled with a saturation current density of $J_o = 1 \times 10^{-13}$ A cm^{-2}. This is representative of a good phosphorus emitter at the front, and of a good aluminum (Al) back surface field (BSF) at the rear. Detailed parameters used for PC1D simulation are shown in Table 2. All these simulations are performed on the samples with three fixed N_A, i. e. 5×10^{16}, 1×10^{17} and 3×10^{17} cm^{-3}.

2.2.1. Short-circuit current

Fig. 7(a) shows the J_{sc} of the solar cells as a function of C_l for three fixed N_A. Generally, the value of J_{sc} increases monotonically with the increase of C_l, which is mainly attributed to the improved L_{diff}. It is worthy of noticing that the J_{sc} shows a relatively weak dependence on the L_{diff} when the L_{diff} is comparable or longer than the solar cell thickness. For instance, in the case of $[B] = 5 \times 10^{16}$ cm^{-3}, the increase of J_{sc} is only 6% when C_l increases from 1 to 199. However, for the solar cells with L_{diff} shorter than the solar cell thickness, the value of J_{sc} could get significantly improved, benefiting from dopant compensation. For instance, the value of J_{sc} increases by 25% in the case of $[B] = 3 \times 10^{17}$ cm^{-3}, when C_l increases from 1 to 199.

Table 2
Device parameters used for PC1D simulation.

Wafer thickness (μm)	200
Device area (cm^2)	148.55
Front surface texture depth (μm)	5
Front surface charge (cm^{-2})	1×10^{12}
Exterior front reflectance	10%
Emitter doping concentration (cm^{-3}) (Gaussian)	1×10^{19}
BSF doping concentration (cm^{-3}) (Uniform)	5×10^{18}
Front surface recombination (A/cm^2, J_o model)	1×10^{-13}
Rear surface recombination (A/cm^2, J_o model)	1×10^{-1}

2.2.2. Open-circuit voltage

Fig. 7(b) shows the V_{oc} of the solar cells as a function of C_l for three fixed N_A. Unlike the J_{sc}, the V_{oc} presents an initial decrease and subsequent increase with the increase of C_l. It is known that the voltage of a front-junction n^+pp^+ device created in a solar cell under illumination is determined by

$$V = \frac{kT}{q} In\left[\frac{(n_o + \Delta n_{front})(p_o + \Delta n_{back})}{n_i^2}\right] \quad (9)$$

where n_i is the intrinsic carrier concentration, Δn_{front} and Δn_{back} are the excess carrier concentrations at the edges of the space-charge regions of the front n^+p junction and the rear pp^+ high–low junction, respectively [10]. Under steady-state conditions, the excess carrier concentration can be derived from the effective minority carrier lifetime by $\Delta n = G\tau_{eff}$, where G is the average carrier generation rate. Dopant compensation not only leads to the reduced p_0 in the silicon base, but also the increased τ_{eff} and therefore the increased Δn. So, with the increase of C_l, the initial

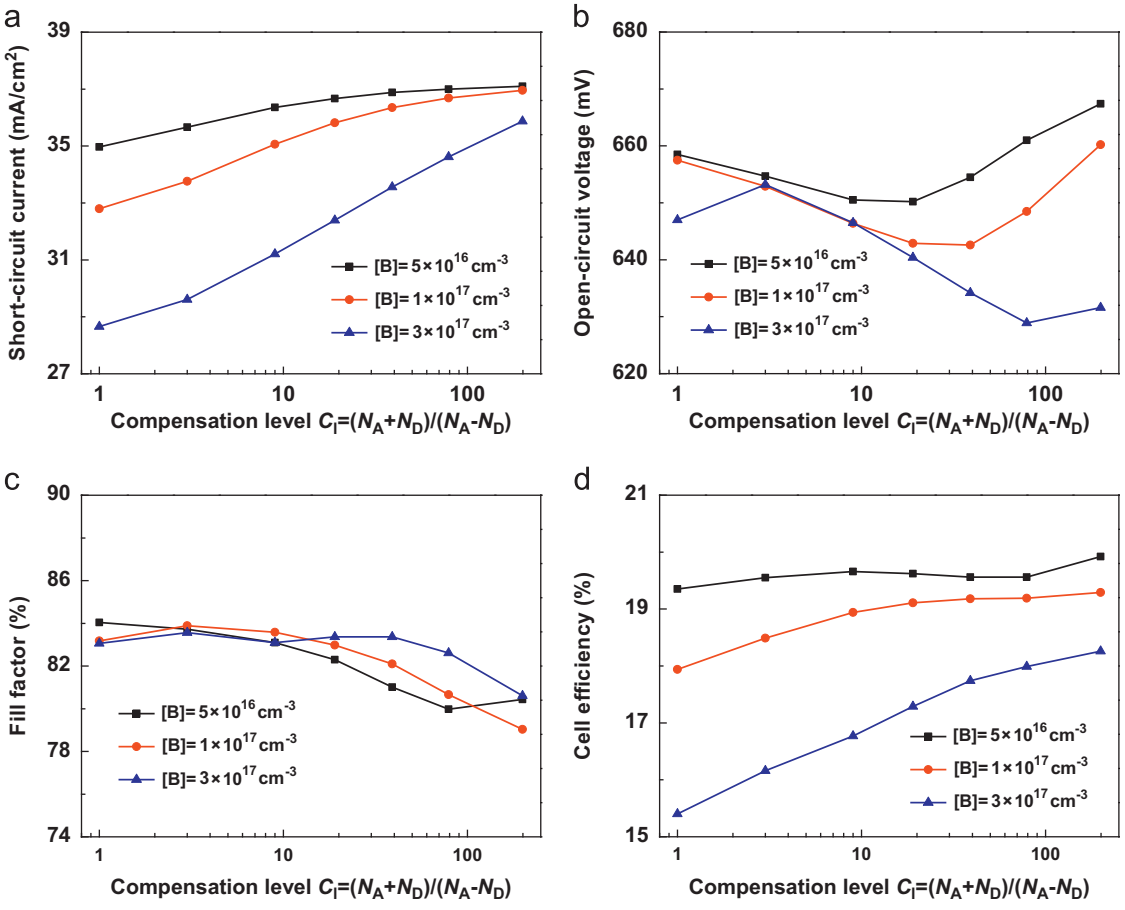

Fig. 7. Electrical parameters of the corresponding solar cells, i. e short-circuit current J_{sc} (a), open-circuit voltage V_{oc} (b), fill factor FF (c) and cell efficiency ŋ (d) as a function of C_l for three fixed N_A.

decrease in the V_{oc} should be attributed to the reduced p_0 in the silicon base, which is associated to the reduced internal *pn* junction barrier height of the corresponding solar cells. Note, a rapid increase in τ_{eff} occurs when C_l reaches a critical value. For instance, in the case of $N_A=5\times10^{16}\,cm^{-3}$, τ_{eff} increases from 21 to 130 μs when C_l increases from 1 to 19, while τ_{eff} increases from 130 to 741 μs when C_l increases from 19 to 199. As a result, when a critical C_l reaches, the increase in the V_{oc} should originate from the large improvement in the τ_{eff}, which could largely counterbalance the reduction of the p_0 in the silicon base.

2.2.3. Fill factor

The *FF* is generally influenced by various factors, i.e. the series and shunt resistances, the V_{oc}, the injection-dependence carrier lifetime effect and the recombination currents within the space charge region [10,13,29]. In our calculations, with C_l increasing, the resistivity of silicon base increases, owing to the reduction of p_0 and μ_h. It gives rise to the increased resistive losses and thus deteriorates the *FF*. Considering that the V_{oc} presents a sectionalized variation trend in our calculations, the situation of C_l dependence on the *FF* could become much more complex, even if the injection-dependence carrier lifetime effect has not been taken into account. However, in many practical cases, the *FF* decreases with C_l increasing [13], see Fig. 7(c). It should be noted that the *FF* values in Fig. 7(c) represent the upper limits which could be achieved in real solar cells, since the resistive losses related to the shunt resistance, the metallization and lateral transport in the emitter have not been taken into consideration.

2.2.4. Cell efficiency

Fig. 7(d) shows the η of the solar cells as a function of C_l for three fixed N_A. It can be seen that in most cases, the η increases monotonically with C_l increasing. Although the V_{oc} presents a downward trend at low C_l and the *FF* generally drops with C_l increasing, the η could get an improvement due to the strongly increased J_{sc}, especially for those cells with highly-doped silicon base. For instance, in the case of $[B]=3\times10^{17}\,cm^{-3}$, the η could increase from 15.4% to 18.3% when C_l increases from 1 to 199. Therefore, for silicon base with the same [*B*], dopant compensation should have a beneficial effect on the cell efficiency. However, we have to mention here that if more P atoms are added into the silicon melt to reach a high C_l in the silicon base, the polarity change from p-type to n-type would occur earlier, due to the segregations of B and P. This would reduce the effective utilization of silicon crystals, which could be overcome by using gallium (Ga) codoping [30].

3. Experimental

3.1. Experimental procedure

To experimentally confirm our theoretically calculated results, one B and P compensated CZ silicon crystal (6 in. diameter) was grown. The [*B*] and [*P*] in the silicon melt are $1.4\times10^{17}\,cm^{-3}$ and $2.4\times10^{17}\,cm^{-3}$, respectively. After crystal growth, 125 mm × 125 mm quasi-square wafers with a thickness of 200 μm were sampled from two parts of the crystal, which correspond to the solidified position fractions of 4.2% and 18.8%, respectively. These two kinds of wafers are labeled as *C*1 and *C*2. The concentrations of interstitial oxygen [Oi] in the *C*1 and *C*2 wafers were determined to be $\sim1.0\times10^{18}\,cm^{-3}$ by a Fourier transform infrared spectroscope (FTIR, Bruker, IFS 66V/S) with a calibration coefficient of $3.14\times10^{17}\,cm^{-2}$. The concentrations of B and P in the *C*1 and *C*2 wafers were calculated from the Sheil laws [31], consistent with the measurement result by a secondary ion mass spectroscopy (SIMS) [13]. The resistivity (ρ) was measured by four-point-probe (FPP) technique after a 650 °C/30 min annealing in Ar ambient to eliminate the grown-in thermal donors (TDs). The μ_h was determined by the combined measurements of ρ and p_0, via $\mu_h=1/q\rho p_0$. The μ_e was obtained by the method of surface-limited effective carrier lifetimes developed by Sproul et al. [32]. More details about the measurement of μ_e can be found in Ref. [13]. Table 3 shows the detailed parameters of the *C*1 and *C*2 wafers. After removing the surface damages, the *C*1 and *C*2 wafers were subjected to a silicon nitride (SiN:H) film deposition for surface passivation by plasma-enhanced chemical vapor deposition (PECVD) technique. The minority carrier lifetime mappings of the *C*1 and *C*2 wafers were performed by a microwave photoconductance decay (MW-PCD) equipment (Semilab WT2000).

Table 3
Detailed parameters of the *C*1 and *C*2 wafers.

Wafer	C_l	N_A (cm^{-3})	N_D (cm^{-3})	p_0 (cm^{-3})	ρ (Ω cm)	μ_p (cm^2/V s)	μ_n (cm^2/V s)
C1	6	1.2×10^{17}	8.6×10^{16}	3.2×10^{16}	1.44 ± 0.05	217 ± 8	597 ± 37
C2	9	1.2×10^{17}	9.6×10^{16}	2.2×10^{16}	2.84 ± 0.04	160 ± 2	565 ± 15

The solar cells based on the *C*1 and *C*2 wafers were fabricated on the same production line at the Trina Solar Company by a standard process, including acid etching, *P* diffusion, SiN_x antireflective coating deposition, screen-printing and contact cofiring. The minority carrier diffusion lengths of these two kinds of solar cells were derived from the short-circuit currents at various near infrared light wavelengths based on the light beam-induced current (LBIC) measurement [33]. The illuminated *I–V* characteristics of solar cells were performed under one sun with AM 1.5 Global spectrum at 25 ± 1 °C prior to any light soaking for the efficiency degradation, using a Berger Flasher PSS 10 solar simulator. The illuminated intensity was calibrated using a reference cell obtained from Fraunhofer ISE, Germany.

3.2. Experimental results

As can be seen from Table 3, the B concentrations in the *C*1 and *C*2 wafers remain constant due to the segregation coefficient of B ($k_B=0.8$) being close to unity, while the P concentrations in the *C*1 and *C*2 wafers have a great difference due to the small segregation coefficient of P ($k_P=0.35$). As a result, the values of C_l in the *C*1 and *C*2 wafers correspond to 6 and 9, respectively. In the case of $[B]=1.2\times10^{17}\,cm^{-3}$, the value of E_B is estimated to ~42.9 meV. The amounts of unionized B atoms in the *C*1 and *C*2 wafers are approximately 2%. As also can be seen from Table 3, the hole mobility in the *C*2 wafer is noticeably lower than that in the C1 wafer, while the electron mobilities in the C1 and *C*2 wafers are almost the same if the uncertainty in the measurement has been taken into account. Fig. 8 presents the effective carrier lifetime mappings of the *C*1 and *C*2 wafers. The average value of the effective carrier lifetime arises from 47.2 μs for the *C*1 wafer to 61.7 μs for the *C*2 wafer. Therefore, it is true that compensation could have a beneficial effect on the effective carrier lifetime. Table 4 summarized the electrical parameters of the *C*1 and *C*2 solar cells. Note that all the data are from the statistic average of 10 solar cells. It can be seen that the minority carrier diffusion length in the *C*2 solar cells is higher than that in the *C*1 solar cells, benefiting from the high effective carrier lifetime. Therefore, the J_{sc} in the *C*2 solar cells is higher than that in the *C*1 solar cells. The V_{oc} in the *C*2 solar cells shows a slightly decrease, which should be attributed to the reduced p_0 in the *C*2 wafers. C_l in the *C*1 and *C*2 wafers correspond to low values, therefore, the p_0 would be

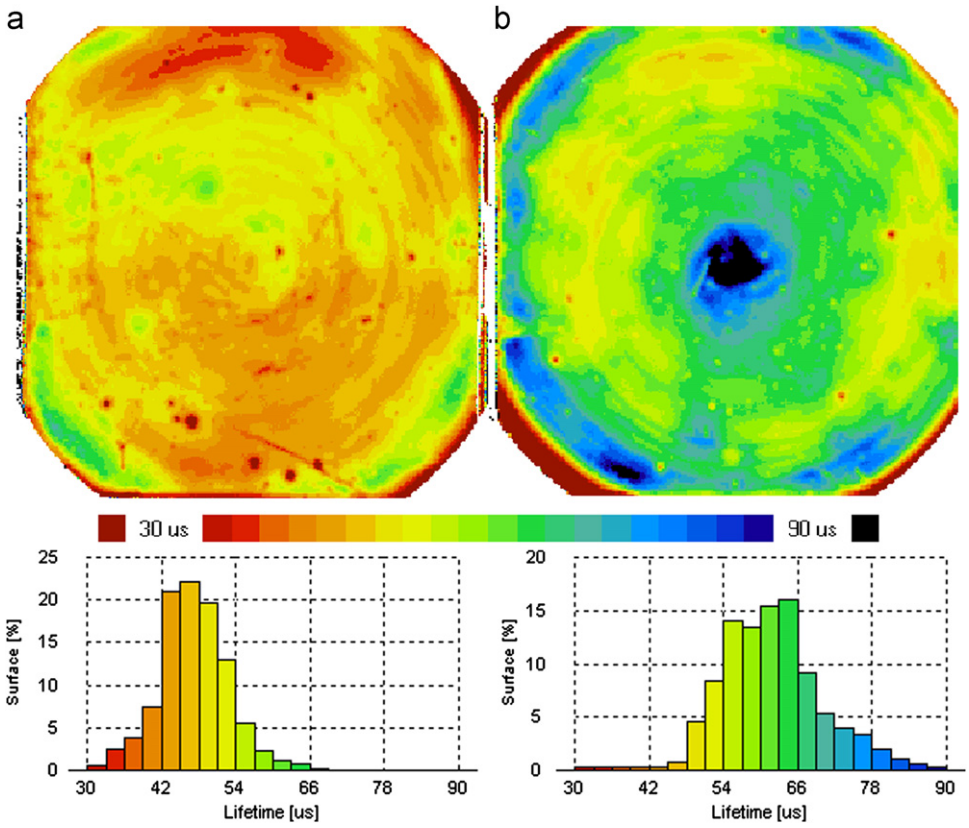

Fig. 8. Effective carrier lifetime mappings of the (a) *C*1 and (b) *C*2 wafers, after removing the surface damages and then wafers are subjected to a silicon nitride (SiN:H) film deposition for surface passivation by plasma-enhanced chemical vapor deposition (PECVD) technique.

Table 4
Electrical parameters of the C1 and C2 solar cells.

Solar cell	L_n (μm)	J_{sc} (mA/cm^2)	V_{oc} (mV)	*FF* (%)	η (%)
C1	358	35.26	632.91	77.7	17.3
C2	423	35.56	632.27	77.5	17.4

the key factor influencing the V_{oc} (see Fig. 7(b)). The *FF* in the *C*2 solar cells also shows a slightly decrease, which might be associated to the reduced V_{oc}. Compared to the *C*1 solar cells, an absolute efficiency gain of ~0.1% has been obtained for the *C*2 solar cells, due to the strongly improved J_{sc}. These experimental results are in good agreement with the theoretically calculated results mentioned above.

It should be mentioned that there is yet no consensus around the validity of standard mobility models in compensated silicon. Our study shows that the minority carrier mobilities are in good agreement with the predicted values based on the Klaassen's model. However, the majority carrier mobilities show a large discrepancy with the predicted values. As solar cells are minority carrier devices, to some degree it is reasonable to use the Klaassen's model in our study. The measured carrier lifetimes are reasonably consistent with the theoretically calculated values in our study. Considering that the electron capture cross section σ_n for B atoms varies from 10^{-17} to10^{-19} cm^2 [9], it is expected that the agreement between the theoretically calculated results and measured results can be further improved by adjusting the recombination parameters. The measured minority carrier diffusion lengths as a function of C_I presents the same trend as the theoretically calculated ones. A little discrepancy between the calculated values and measured values should mainly originate from two aspects. One is that the measured carrier lifetimes have a little difference with the calculated ones, as mentioned above. The other is the non-linear effect of cell fabrication process on the electrical properties of silicon material [24]. In practice, the final carrier lifetime measured on a solar cell might differ from the carrier lifetime measured on silicon wafer. Therefore, the measured minority carrier diffusion lengths would have a slightly small difference with the calculated ones.

4. Conclusions

In summary, we have investigated the influence of C_I on the performance of crystalline silicon solar cells by means of theoretical calculations and experiments. It is found that with C_I increasing, the fraction of ionized B atoms would increase, while the incomplete ionization ratio almost keeps constant. Due to the increased ionized acceptor and donor impurities scattering, the hole mobility is significantly reduced by the dopant compensation. However, the electron mobility almost remains constant in p-type silicon with the same [*B*], due to the inverse contributions of ionized acceptor and donor impurities scatting and electron–hole scattering. Taking into accounting the influence of both B and FeB pairs on the carrier lifetime, it is found that the carrier lifetime in silicon wafer is mainly dominated by the high concentration of dopants, rather than the low concentration of metal impurities after a PDG process. Moreover, with C_I increasing, the carrier lifetimes limited by both B and FeB pairs could get improved, which results in the increased effective carrier lifetime, the increased minority carrier diffusion length and therefore the increased J_{sc}. Nevertheless, the V_{oc} is mainly dependent on the competition effect of the reduced p_0 and the increased excess carrier concentration. At low C_I, the reduced p_0 is the key factor

which results in the reduced V_{oc}, while at high C_I the increased excess carrier concentration becomes the important factor which leads to the increased V_{oc}. In most cases, the *FF* decreases with C_I increasing. However, due to the strongly improved J_{sc}, the η of the final solar cells could get improved, especially for those cells with highly-doped silicon feedstock. These results suggest that intentional dopant compensation might become a promising way to the improvement of solar cell efficiency without increasing cost. It is quite meaningful for the wide application of UMG-Si feedstock in PV industry.

Acknowledgments

This work is supported by National Natural Science Foundation of China (Nos. 60906002 and 50832006), National Key Technology R&D Program (2011BAE03B13), and Innovation Team Project of Zhejiang Province (2009R50005). The authors thank Trina Company for the fabrication of solar cells and the related measurement.

References

[1] N. Yuge, H. Baba, Y. Sakaguchi, K. Nishikawa, H. Terashima, F. Aratani, Purification of metallurgical silicon up to solar grade, Solor Energy Materials and Solar Cells 34 (1994) 243–250.
[2] C. Alemany, C. Trassy, B. Pateyron, K.-I. Li, Y. Delannoy, Refining of metallurgical-grade silicon by inductive plasma, Solor Energy Materials and Solar Cells 72 (2002) 41–48.
[3] Y. Delannoy, C. Alemany, K.-I. Li, P. Proulx, C. Trassy, Plasma-refining process to provide solar-grade silicon, Solor Energy Materials and Solar Cells 72 (2002) 69–75.
[4] J.C.S. Pires, J. Otubo, A.F.B. Braga, P.R. Mei, The purification of metallurgical grade silicon by electron beam melting, Journal of Materials Processing Technology 169 (2005) 16–20.
[5] G. Flamant, V. Kurtcuoglu, J. Murray, A. Steinfeld, Purification of metallurgical grade silicon by a solar process, Solor Energy Materials and Solar Cells 90 (2006) 2099–2106.
[6] A.F.B. Braga, S.P. Moreira, P.R. Zampieri, J.M.G. Bacchin, P.R. Mei, New processes for the production of solar-grade polycrystalline silicon: a review, Solor Energy Materials and Solar Cells 92 (2007) 418–424.
[7] F.E. Rougieux, D. Macdonald, A. Cuevas, S. Ruffell, J. Schmidt, B. Lim, A.P. Knights, Electron and hole mobility reduction and hall factor in phosphorus-compensated p-type silicon, Journal of Applied Physics 108 (2010) 013706-1–013706-5.
[8] F.E. Rougieux, D. Macdonald, A. Cuevas, Transport properties of p-type compensated silicon at room temperature, Progress in Photovoltaics: Research and Applications 19 (2011) 787–793.
[9] S. Dubois, N. Enjalbert, J.P. Garandet, Effect of the compensation level on the carrier lifetime of crystalline silicon, Applied Physics Letters 93 (2008) 032114-1–032114-3.
[10] D. Macdonald, A. Cuevas, Recombination in compensated crystalline silicon for solar cells, Journal of Applied Physics 109 (2011) 043704-1–043704-8.
[11] J. Libal, S. Novaglia, M. Acciarri, S. Binetti, R. Petres, J. Arumughan, R. Kopecek, A. Prokopenko, Effect of compensation and of metallic impurities on the electrical properties of CZ-grown solar grade silicon, Journal of Applied Physics 104 (2008) 104507-1–104507-8.
[12] J. Veirman, S. Dubois, N. Enjalbert, J.–P. Garandet, M. Lemiti, Electronic properties of highly-doped and compensated solar-grade silicon wafers and solar cells, Journal of Applied Physics 109 (2011) 103711-1–103711-10.
[13] C.Q. Xiao, D.R. Yang, X.G. Yu, P. Wang, P. Chen, D.L. Que, Effect of dopant compensation on the performance of Czochralski silicon solar cells, Solar Energy Materials and Solar Cells 101 (2012) 102–106.
[14] M. Forster, A. Cuevas, E. Fourmond, F.E. Rougieux, M. Lemiti, Impact of incomplete ionization of dopants on the electrical properties of compensated p-type silicon, Journal of Applied Physics 111 (2012) 043701-1–043701-7.
[15] P.P. Altermatt, A. Schenk, B. Schmithusen, G. Heiser, A simulation model for the density of states and for incomplete ionization in crystalline silicon. II. Investigation of Si:As and Si:B and usage in device simulation, Journal of Applied Physics 100 (2006) 113715-1–113715-7.
[16] M. Tajima, T. Iwai, H. Toyota, S. Binetti, D. Macdonald, Donor-acceptor pair luminescence in compensated Si for solar cells, Journal of Applied Physics 110 (2011) 043506-1–043506-5.
[17] D. Arora, R. Hauser, J. Roulston, Electron and hole mobilities in silicon as a function of concentration and temperature, IEEE Transactions on Electron Devices 2 (1982) 292–295.
[18] W.R. Thurber, R.L. Mattis, Y.M. Liu, J.J. Filliben, Resistivity-dopant density relationship for boron-doped silicon, Journal of the Electrochemistry Society 127 (1980) 2291–2294.
[19] W.R. Thurber, R.L. Mattis, Y.M. Liu, J.J. Filliben, Resistivity-dopant density relationship for phosohorus-doped silicon, Journal of the Electrochemistry Society 127 (1980) 1807–1812.
[20] J.M. Dorkel, P. Leturcq, Carrier mobilites in silicon semi-empirically related to temperature, doping and injection level, Solid-State Electronics 24 (1981) 821–825.
[21] D.B.M. Klaassen, A unified mobility model for device calculation-I. Model equations for and concentration dependence, Solid-State Electronics 35 (1992) 953–959.
[22] D.B.M. Klaassen, A unified mobility model for device calculation-I. Temperature dependence of carrier mobility and lifetime, Solid-State Electronics 35 (1992) 961–967.
[23] W. Shockley, W.T. Read, Statistics of the recombinations of holes and electrons, Physical Review 87 (1952) 835–842.
[24] J. Hofstetter, D.P. Fenning, M.I. Bertoni, J.F. Lelievre, C. del Canizo, T. Buonassisi, Impurity-to-efficiency simulator: predictive calculation of silicon solar cell performance based on iron content and distribution, Progress in Photovoltaics: Research and Applications 19 (2011) 487–497.
[25] V. Vahanissi, A. Haarahiltunen, H. Talvitie, M. Yli-Koski, H. Savin, Impact of phosphorus gettering parameters and initial iron level on silicon solar cell properties, Progress in Photovoltaics: Research and Applications, in press, http://dx.doi.org/10. 1002/ pip. 2215.
[26] D. Macdonald, T. Roth, P.N.K. Deenapanray, T. Trupke, R.A. Bardos, Doping dependence of the carrier lifetime crossover point upon dissociation of iron–boron pairs in crystalline silicon, Applied Physics Letters 89 (2006) 142107-1–142107-3.
[27] D. Macdonald, A. Cuevas, Validity of simplified Shockley-Read-Hall statistics for modeling carrier lifetimes in crystalline silicon, Physical Review B 67 (2003) 075203-1–075203-7.
[28] P.A. Basore, D.A. Clugston, PC1D V5.9, University of New South Wales, 2003.
[29] M. Green, Solar Cells Operating Principles, Technology and System Applications, 78, University of New South Wales, Kensington, 1982, pp. 96–98.
[30] M. Forster, E. Fourmond, R. Einhaus, H. Lauvray, J Kraiem, M. Lemiti, Ga co-doping in Cz-grown silicon ingots to overcome limitations of B and P compensated silicon feedstock for PV applications, Physics Status Solidi C 8 (2011) 678–681.
[31] E. Sheil, Zeitschrift für Metallkunde 34 (1942) 70–72.
[32] A.B. Sproul, M.A. Green, A.W. Stephens, Accurate determination of minority carrier- and lattice scattering-mobility in silicon from photoconductance decay, Journal of Applied Physics 72 (1992) 4161–4171.
[33] E.D. Stokes, T.L. Chun, Diffusion lengths in solar cells from short-circuit current measurement, Applied Physics Letters 30 (1977) 425–426.